

Half-range lattice Boltzmann models for the simulation of Couette flow using the Shakhov collision term

Victor E. Ambrus^{1,2,*} and Victor Sofonea^{1,†}

¹*Center for Fundamental and Advanced Technical Research,
Romanian Academy, Bd. Mihai Viteazul 24, 300223 Timișoara, Romania*

²*Department of Physics, West University of Timișoara,
Bd. Vasile Pârvan 4, 300223 Timișoara, Romania*

(Dated: December 3, 2024)

Abstract

The three-dimensional Couette flow between parallel plates is addressed using mixed lattice Boltzmann models which implement the half-range and full-range Gauss-Hermite quadratures on the Cartesian axes perpendicular and parallel to the walls, respectively. Our models are validated through a comparison against previously reported results obtained using the linearised Boltzmann equation for values of the Knudsen number (Kn) up to 100. Furthermore, an adequate application of the Shakhov collision term allows our models to recover DSMC results for the temperature profile for Kn up to 1.0. Finally, we employ a convergence test to show that our quadrature procedure allows the simulation errors to decrease smoothly when the quadrature order is increased. We find that for low speed flows (when the non-dimensional wall velocities are ± 0.1), 108 velocities are sufficient to reduce the errors in the profiles of the particle number density, velocity, temperature and heat fluxes below 1% compared to our reference model, from the Navier-Stokes regime (low Kn) up to the ballistic regime ($\text{Kn} \rightarrow \infty$).

* E-mail: victor.ambrus@e-uvvt.ro

† E-mail: sofonea@acad-tim.tm.edu.ro

I. INTRODUCTION

In the Navier-Stokes regime, it is known that the BGK approximation for the collision term is not appropriate for the realistic simulation of dissipative flows. Indeed, a Chapman-Enskog analysis shows that the Prandtl number Pr in the BGK approximation is equal to unity [1] while for hard-sphere particles, it should be equal to $2/3$. In order to achieve the correct value for Pr in the Navier-Stokes regime, in our lattice Boltzmann (LB) models we employ the Shakhov collision term [2–8]. This collision term allows Pr to be controlled as an independent quantity by modifying the thermal conductivity κ_T . We will show that setting $Pr = 2/3$ through this mechanism allows the Direct Simulation Monte Carlo (DSMC) data obtained for the Couette flow of hard sphere particles [9–13] to be reproduced for small Kn . As Kn is increased, the concept of transport coefficients is ambiguous, since the constitutive equations of the Newtonian fluid, as well as Fourier’s law for heat transfer, are no longer applicable. In the rarefied regime, Pr becomes just a parameter of the Shakhov model. We find that our simulation results match the DSMC data beyond the hydrodynamic regime only after adjusting the value of the Pr parameter [14].

In this paper, we only discuss the Couette flow between parallel plates. At non-negligible values of Kn , the diffuse reflection boundary conditions imposed on the plates induce a discontinuity in the distribution function [15]. For this reason, appropriate half-range quadratures should be employed on the direction perpendicular to the walls [4–6, 8, 16–29] in order to obtain accurate results using the LB models. In order to reduce the number of the discrete velocity vectors, in this paper we will employ the mixed quadrature LB models introduced in Ref. [28] for the study of the 2D Couette flow.

Since we are interested in obtaining accurate results for the temperature field, as well as for the heat flux, the number of degrees of freedom in the momentum space must be equal to three. This requires the extension of the models introduced in Ref. [28] to three momentum space dimensions. Since these models are based on a direct product of one-dimensional quadratures, their extension to 3D is straightforward. The ensuing models employ the half-range Gauss-Hermite quadrature on the axis perpendicular to the walls (the x axis) and the full-range Gauss-Hermite quadrature for the axes parallel to the walls (the y and z axes). The advantage of this quadrature method is described as follows. The discontinuity induced by the diffuse reflection boundary conditions imposed on the walls perpendicular to the x

axis warrants the use of the half-range Gauss-Hermite quadrature, which requires $Q = N + 1$ points on each Cartesian semiaxis to ensure N th order accuracy. The $2Q$ quadrature points on the whole axis are twice the number of points required by the full-range Gauss-Hermite quadrature to achieve the same degree of accuracy [28]. Thus, it is more convenient to employ the full-range Gauss-Hermite quadratures on the y and z directions (i.e., the directions parallel to the walls), where no discontinuities in the distribution function arise, resulting in an overall smaller velocity set.

The aim of this paper is to demonstrate that the Shakhov model can be successfully employed to match the DSMC simulation results. While this is clearly possible in the hydrodynamic regime by setting the Prandtl number $\text{Pr} = 2/3$, at large values of the relaxation time we highlight that by adjusting the parameter Pr , the DSMC results for hard spheres can be very accurately recovered. This is remarkable since the Shakhov model is in essence a single relaxation time model with one free parameter (i.e. Pr), while the DSMC method implements an equivalent of the Boltzmann collision integral. Even though the value of Pr required to fit the DSMC data at a given Kn number also depends on the magnitude of the wall velocity, we still find it remarkable that the DSMC data can be reproduced within the Shakhov model even for flows where $\text{Kn} = 1.0$ and the wall velocity is $u_w = \pm 2.1$ (500 m/s).

The outline of this paper is as follows. In Sec. II, the Shakhov collision term is briefly described. Section III is dedicated to discussing the Boltzmann equation for the 3D Couette flow between parallel plates. Section IV validates our models by comparing our results with the results obtained for the slip velocity obtained using the linearised Boltzmann equation [30, 31], as well as with the results obtained for the non-hydrodynamic part of the velocity profile reported in Ref. [32]. Also, the comparison with the DSMC data of Refs. [9–13] is shown in this section. Section V discusses the convergence properties of our models with respect to the quadrature order employed for the whole spectrum of Kn . Section VI ends this paper with conclusions. For the reader’s convenience, Appendix A provides the necessary details regarding the non-dimensionalisation of the Boltzmann equation such that our simulations can be performed at the same parameters as the DSMC simulations in Ref. [13]. Finally, Appendix B presents an analysis of the number of iterations required to achieve the steady-state solution when simulating the Couette flow in the Navier-Stokes regime.

II. BOLTZMANN EQUATION WITH THE SHAKHOV COLLISION TERM

The Boltzmann equation for a force-free flow with the Shakhov collision term [2, 3, 25, 33–35], non-dimensionalised as presented in Appendix A, reads:

$$\partial_t f + \frac{\mathbf{p}}{m} \nabla f = -\frac{1}{\tau} [f - f^{(\text{eq})} (1 + \mathbb{S})], \quad (2.1)$$

where f is the Boltzmann distribution function, \mathbf{p} is the particle momentum vector, $f^{(\text{eq})}$ is the Maxwell-Boltzmann equilibrium distribution function (A5), τ is the relaxation time given in Eq. (A6) and \mathbb{S} is given by:

$$\mathbb{S} = \frac{1 - \text{Pr}}{nT^2} \left(\frac{\boldsymbol{\xi}^2}{5mT} - 1 \right) \mathbf{q} \cdot \boldsymbol{\xi}. \quad (2.2)$$

In the above, Pr gives the Prandtl number (see below), $\boldsymbol{\xi} = \mathbf{p} - m\mathbf{u}$ is the peculiar momentum, while the heat flux \mathbf{q} is obtained as a moment of f :

$$\mathbf{q} = \int d^3p \frac{\boldsymbol{\xi}^2}{2m} \frac{\boldsymbol{\xi}}{m} f. \quad (2.3)$$

By employing the Chapman-Enskog expansion, it can be seen that, for three-dimensional flows, the Shakhov collision term gives rise to the following expressions for the transport coefficients, namely, the dynamic (shear) viscosity η and the heat conductivity κ_T [35]:

$$\eta = \tau n T, \quad \kappa_T = \frac{1}{\text{Pr}} \frac{5}{2m} \tau n T, \quad (2.4)$$

where the Prandtl number Pr, calculated as

$$\text{Pr} = \frac{c_p \eta}{\kappa_T}, \quad c_p = \frac{5}{2m}, \quad (2.5)$$

is adjustable according to Eq. (2.2). The local macroscopic moments appearing above, namely, the particle number density n , the fluid velocity \mathbf{u} and the temperature T , are obtained as moments of f , as follows:

$$n = \int d^3p f, \quad (2.6a)$$

$$\mathbf{u} = \frac{1}{n} \int d^3p f \mathbf{p}, \quad (2.6b)$$

$$T = \frac{2}{3n} \int d^3p f \frac{\boldsymbol{\xi}^2}{2m}, \quad (2.6c)$$

while \mathbf{q} is given in Eq. (2.3).

III. LATTICE BOLTZMANN MODELS FOR THE COUETTE FLOW

For the remainder of this paper, we shall focus on the Couette flow between parallel plates. The coordinate system is chosen such that the x axis is perpendicular to the plates, which are located at $x_{\text{left}} = -L/2$ and $x_{\text{right}} = L/2$. The plates are set in motion along the y direction with constant velocity $u_{\text{left}} = -u_w$ and $u_{\text{right}} = u_w$, while their temperature is kept constant at $T_{\text{left}} = T_{\text{right}} = T_w$.

In order to simulate the above flow, we employ the lattice Boltzmann models presented in Ref. [28]. While these models were used in Ref. [28] for the simulation of the 2D Couette flow in the Boltzmann-BGK model, their extension to the 3D case considered here is straightforward. It was shown in Ref. [28] that, for the simulation of flows at non-negligible values of Kn, the half-range Gauss-Hermite quadrature should be used on the axis perpendicular to the walls (the x axis), while a relatively low-order full-range Gauss-Hermite quadrature is adequate for the directions parallel to the walls. We shall denote the resulting models by $\text{HHLB}(Q_x) \times \text{HLB}(Q_y) \times \text{HLB}(Q_z)$, where Q_x denotes the quadrature order employed on each x semiaxis and Q_y and Q_z denote the quadrature orders employed on the full y and z axes. The resulting velocity set comprises $2Q_x \times Q_y \times Q_z$ vectors and is the 3D extension of the 2D velocity set employed in Refs. [28, 29].

In Ref. [28] it was shown, for a two-dimensional mixed quadrature LB model, that the value of Q_x required to obtain accurate simulation results depends on Kn and on the wall velocity u_w . Furthermore, it was also shown that, in the particular case of the BGK implementation of the collision term, the simulations employing $Q_y \geq 4$ at fixed Q_x produced identical results. In this section, a similar inequality will be determined in the 3D case for the quadrature orders Q_y and Q_z corresponding to the axes parallel to the walls.

Since the Couette flow is completely homogeneous along the directions which are parallel to the walls (i.e. the y and z directions), Eq. (2.1) reduces to:

$$\partial_t f + \frac{p_x}{m} \partial_x f = -\frac{1}{\tau} [f - f^{(\text{eq})}(1 + \mathbb{S})], \quad (3.1)$$

Let us now expand f and $f^{(\text{eq})}(1 + \mathbb{S})$ with respect to the full-range Hermite polynomials on

the y and z momentum axes, as follows [36]:

$$f = \frac{\omega(\bar{p}_y)}{p_{0,y}} \frac{\omega(\bar{p}_z)}{p_{0,z}} \sum_{\ell=0}^{\infty} \frac{1}{\ell!} \sum_{s=0}^{\infty} \frac{1}{s!} \mathcal{F}_{\ell s}(x, p_x, t) H_{\ell}(\bar{p}_y) H_s(\bar{p}_z),$$

$$f^{(\text{eq})} (1 + \mathbb{S}) = \frac{\omega(\bar{p}_y)}{p_{0,y}} \frac{\omega(\bar{p}_z)}{p_{0,z}} \sum_{\ell=0}^{\infty} \frac{1}{\ell!} \sum_{s=0}^{\infty} \frac{1}{s!} \mathcal{F}_{\ell s}^{\mathbb{S}}(x, p_x, t) H_{\ell}(\bar{p}_y) H_s(\bar{p}_z), \quad (3.2)$$

where $\bar{p}_{\alpha} \equiv p_{\alpha}/p_{0,\alpha}$ ($\alpha \in \{x, y, z\}$) is the α component of the momentum vector \mathbf{p} , nondimensionalised with respect to the α component $p_{0,\alpha}$ of some reference momentum vector \mathbf{p}_0 .

The weight function $\omega(x)$ for the full-range Hermite polynomials is

$$\omega(\bar{p}_{\alpha}) = \frac{1}{\sqrt{2\pi}} e^{-\bar{p}_{\alpha}^2/2}. \quad (3.3)$$

Furthermore, the coefficients $\mathcal{F}_{\ell s}$ and $\mathcal{F}_{\ell s}^{\mathbb{S}}$ can be computed as:

$$\mathcal{F}_{\ell s} = \int_{-\infty}^{\infty} dp_y \int_{-\infty}^{\infty} dp_z f H_{\ell}(\bar{p}_y) H_s(\bar{p}_z),$$

$$\mathcal{F}_{\ell s}^{\mathbb{S}} = \int_{-\infty}^{\infty} dp_y \int_{-\infty}^{\infty} dp_z f^{(\text{eq})} (1 + \mathbb{S}) H_{\ell}(\bar{p}_y) H_s(\bar{p}_z). \quad (3.4)$$

The compatibility between Eqs. (3.2) and (3.4) is ensured by the orthogonality relation obeyed by the Hermite polynomials [37]:

$$\int_{-\infty}^{\infty} dx \omega(x) H_{\ell}(x) H_{\ell'}(x) = \ell! \delta_{\ell\ell'}. \quad (3.5)$$

Substituting Eqs. (3.2) into the Boltzmann equation (3.1) and projecting on the space of Hermite polynomials gives:

$$\partial_t \mathcal{F}_{\ell s} + \frac{p_x}{m} \partial_x \mathcal{F}_{\ell s} = -\frac{1}{\tau} (\mathcal{F}_{\ell s} - \mathcal{F}_{\ell s}^{\mathbb{S}}), \quad (3.6)$$

where, as before, $\mathcal{F}_{\ell s}$ and $\mathcal{F}_{\ell s}^{\mathbb{S}}$ depend on x , p_x and t . Since $f^{(\text{eq})}$ depends on n , \mathbf{u} and T , while \mathbb{S} depends on \mathbf{q} , the coefficients $\mathcal{F}_{\ell s}^{\mathbb{S}}$ always involve the coefficients $\mathcal{F}_{\ell' s'}$ of orders $0 \leq \ell' \leq 3$ and $0 \leq s' \leq 3$. Moreover, since q_z is always 0, only the coefficients with $0 \leq s' \leq 2$ are relevant for the construction of $\mathcal{F}_{\ell s}^{\mathbb{S}}$. Thus, the Boltzmann equation (3.1) can be truncated at order N with respect to the Hermite basis on the p_y and p_z axes.

The order of the full-range Hermite quadratures on the y and z axes can be determined as follows. Since in this paper, only the moments of f up to \mathbf{q} are tracked, we are only interested in the evolution of the coefficients $\mathcal{F}_{\ell s}$ with $0 \leq \ell, s \leq 3$. In our implementation, we consider the expansion of $f^{(\text{eq})}$ with respect to Hermite polynomials, as follows:

$$f^{(\text{eq})} = n g_x g_y g_z, \quad g_{\alpha} = \frac{1}{\sqrt{2\pi m T}} \exp \left[-\frac{(p_{\alpha} - m u_{\alpha})^2}{2mT} \right], \quad (3.7)$$

where g_x is expanded with respect to the half-range Hermite polynomials and g_y and g_z are expanded with respect to the full-range Hermite polynomials up to orders $N_y = Q_y - 1$ and $N_z = Q_z - 1$, respectively [28, 29]. Since \mathbb{S} is a polynomial of the third order in \mathbf{p} , the evolution of \mathbf{q} requires the recovery of the moments of $f^{(\text{eq})}$ of order $3 + 3 = 6$ on each axis. Such moments can be exactly recovered when $N_y \geq 6$ and $N_z \geq 6$.

The above analysis shows that, when the Shakhov collision term is employed, the numerical results for the 3D Couette flow considered in this paper when $Q_y, Q_z > 7$ must coincide with those obtained with $Q_y = Q_z = 7$. Furthermore, as discussed in Ref. [28], the accurate simulation of flows at large values of Kn requires the increase of the quadrature Q_x . In this paper, we follow Ref. [28] and choose the profiles obtained using the HHLB(21) \times HLB(7) \times HLB(7) model (corresponding to $Q_x = 21$) as the reference profiles which will make the subject of the following section. In Sec. V, we will show the convergence trend of our models as Q_x is increased towards 21 by employing the convergence test introduced in Refs. [28, 29].

Before ending this section, it is worth mentioning that if $\text{Pr} = 1$, the Shakhov term \mathbb{S} in Eq. (2.2) vanishes and the LB models with $Q_y, Q_z \geq 4$ give identical results, as discussed in Ref. [28].

IV. REFERENCE PROFILES

In this section, the reference profiles obtained using the HHLB(21) \times HLB(7) \times HLB(7) model are validated against the results obtained using other numerical methods. The numerical results presented in this section were obtained on a lattice of $128 \times 1 \times 1$ nodes in the x , y and z directions, respectively. The time step δt was set to 5×10^{-4} for $\text{Kn} \geq 0.1$, while for $\text{Kn} < 0.1$, the time step was decreased to $\delta t = 1 \times 10^{-4}$ in order to reduce the effect of numerical errors and to avoid the collision term becoming stiff.

Next, we will present some information regarding the number of iterations that we performed to achieve the stationary state.

At $0.001 < \text{Kn} < 0.1$, the flow is close to the inviscid limit and an analytic analysis (see Appendix B) indicates that a number of 10^6 iterations must be performed to achieve the steady state. For large values of Kn, the ballistic regime sets in, where the time scale on which the flow becomes stationary is that required by the particles in the initial state to reach

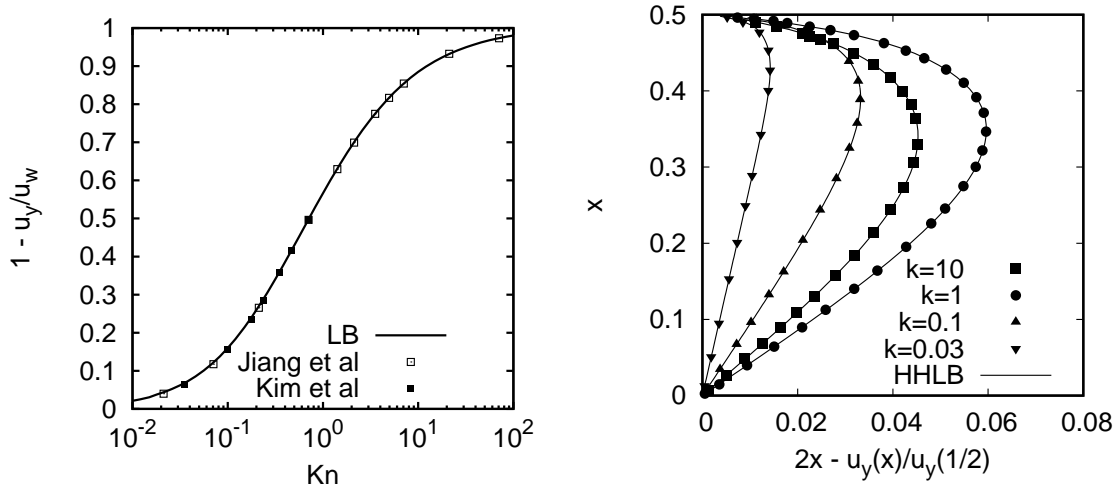


FIG. 1. Comparison between the results obtained using our models and: (a) The linearised Boltzmann equation for the slip velocity reported in Refs. [31] and [30]; (b) The non-hydrodynamic part of the velocity profile reported in Ref. [32].

the boundary walls. For a quadrature order $Q_x = 21$, the slowest particle has $p_x \simeq 0.0188$, requiring a time $\Delta t \simeq 53.2$ to cross the unit-length channel. Since $\delta t = 5 \times 10^{-4}$, a number of $\sim 106,383$ iterations are required for this particle to cross the channel. Thus, for all $Kn \geq 1$, we always performed 200,000 iterations.

When $0.1 \leq Kn < 1.0$, the flow is neither in the inviscid regime nor in the ballistic regime. At $Kn = 0.1$, Eq. (B12) implies that a number of 10,000 iterations should suffice to achieve the steady state. We found that, for the above range of Kn , 60,000 iterations were sufficient for the flow to become stationary.

For the spatial advection, we employed the second order flux limiter scheme described in Refs. [28, 29], while the time stepping was performed using a third-order Runge-Kutta algorithm [38]. The implementation of the diffuse reflection boundary conditions on the channel walls is identical to that presented in Refs. [28, 29].

In Figure 1(a), we present a comparison between the results obtained using our reference model and those obtained using the linearised Boltzmann equation in Ref. [30], as well as the benchmark results published in Ref. [31], for the velocity slip u_{slip} , defined as follows:

$$u_{\text{slip}} = u_w - u(x = L/2). \quad (4.1)$$

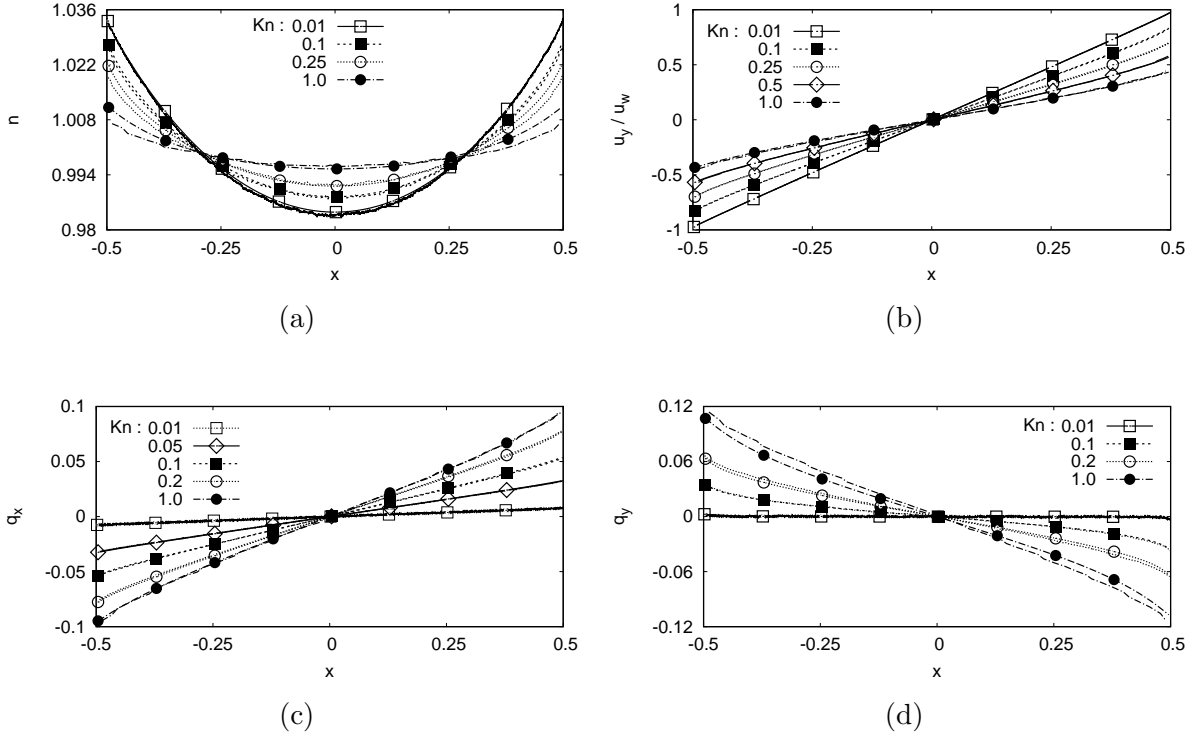


FIG. 2. Reference profiles of the (a) density n , (b) normalised longitudinal velocity u_y/u_w , (c) transverse heat flux q_x and (d) longitudinal heat flux q_y , obtained using the HHLB(21) \times HLB(7) \times HLB(7) model, corresponding to the Couette flow between parallel plates at temperature $T_w = 1.0$ and velocity $u_w = 0.63$. The LB results (lines and points) for various values of the Knudsen number Kn are compared to the corresponding DSMC results (lines only) presented in Ref. [9]. The same type of line is used to plot both the LB and the DSMC results for each Kn .

In order to compare with the results in Ref. [30], the Knudsen number introduced therein was multiplied by a factor of $\sqrt{2/\pi}$, i.e. $Kn \rightarrow Kn\sqrt{2/\pi}$. Similarly, the Knudsen number employed in Ref. [31] was rescaled using a factor of $1/\sqrt{2}$.

The results presented in Fig. 1(a) were obtained for $u_w = 0.1$. At higher values of u_w , the LB results present slight deviations from the benchmark results. This is to be expected, since the profile of u_y/u_w does not scale perfectly with u_w , as also demonstrated in Ref. [39]. It is remarkable that the velocity profiles obtained using our models do not seem to depend on the value of Pr . In particular, the BGK collision term and the Shakhov collision term with $Pr = 2/3$ and with $Pr = 4/3$ yield identical results. It can be seen that the agreement between our results and those reported in Refs. [30, 31] is very good.

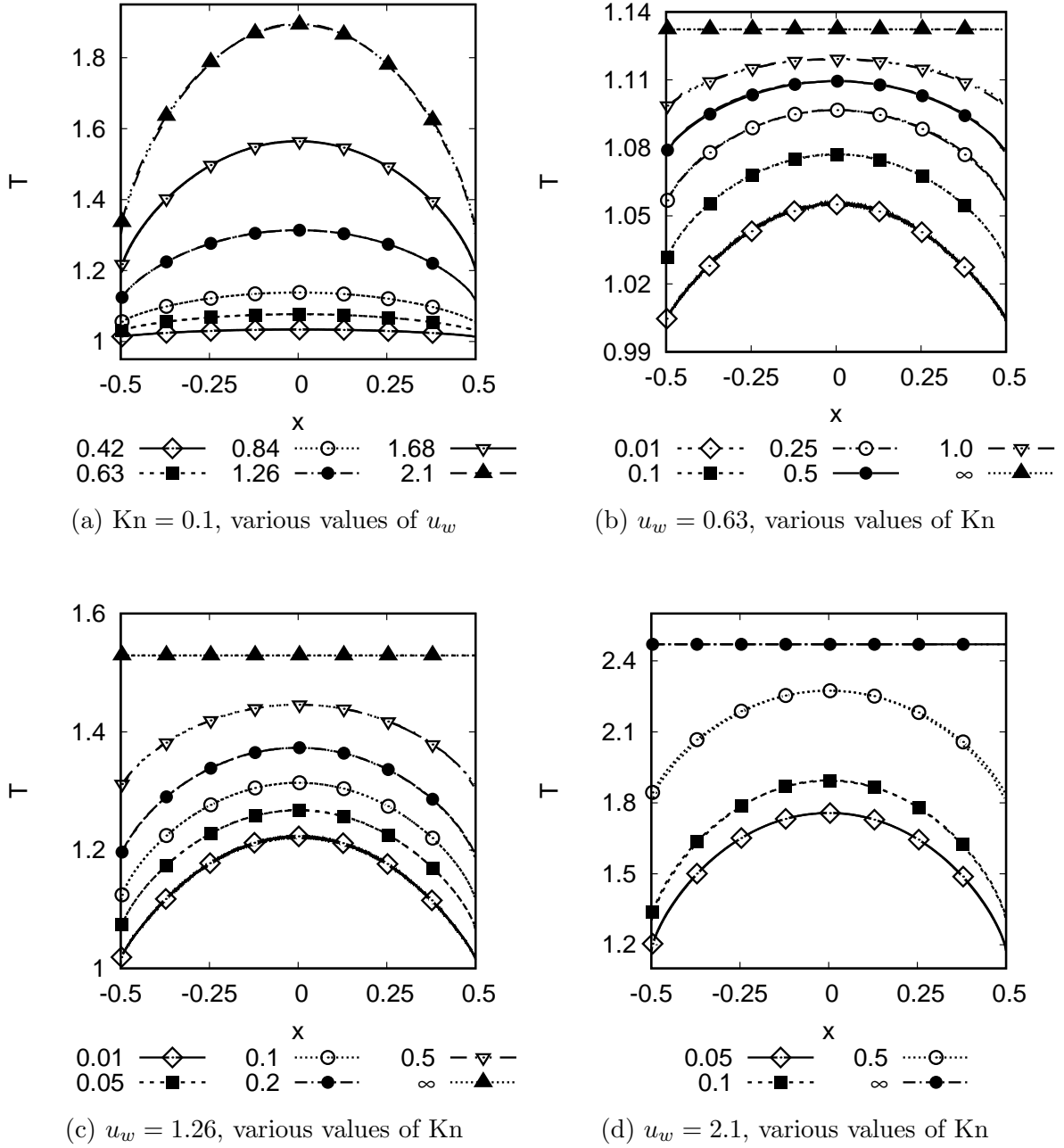


FIG. 3. Comparison between the temperature profiles obtained using the $\text{HHLB}(21) \times \text{HLB}(7) \times \text{HLB}(7)$ model (lines and points) and the DSMC results (lines) reported in Ref. [13]: (a) $\text{Kn} = 0.1$ and various values of the plate velocity u_w ; (b) $u_w = 0.63$ and various values of Kn ; (c) same, with $u_w = 1.26$; (d) same, with $u_w = 2.1$. In (b), (c) and (d), the LB results obtained in the ballistic limit are compared with the analytic result (4.3).

In Fig. 1(b), we analyse the non-hydrodynamic part of the velocity profile, defined as:

$$2x - \frac{u_y(x)}{u_y(1/2)}. \quad (4.2)$$

The above expression subtracts the velocity profile $u_y(x)$ from the hydrodynamic solution $u_y^{\text{hydro}} = 2xu_y(1/2)$, which takes into account the correct slip velocity. The result is normalised with respect to the velocity on the wall. The resulting profile cancels at the centre of the channel and on the wall and reaches a maximum value inside the channel. The value of this maximum increases with $k = \text{Kn}\sqrt{2}$ up to a maximum value, and decreases afterwards as $k \rightarrow \infty$, when the velocity profile is trivially a straight line: $u_y^{\text{bal}}(x) = 0$. Since the results reported in Ref. [32] were obtained in the linearised regime, we set the velocity of the walls to $u_w = \pm 0.001$. At such a low Mach number, the flow is incompressible and isothermal. Our simulation results were obtained using the models $\text{HHLB}(Q_x) \times \text{HLB}(2) \times \text{HLB}(2)$, where $Q_x = 4, 11, 21$ and 100 for $k = 0.03, 0.1, 1$ and 10 . The agreement between our simulation results and the benchmark results of Ref. [32] is excellent.

Next, we considered a comparison against the Direct Simulation Monte Carlo (DSMC) results reported in [13], and also in Refs. [9–12]. The correspondence between our simulation parameters and the quantities employed in the DSMC simulations was taken into account in the non-dimensionalisation procedure, which we discuss in Appendix A.

Fig. 2 shows a comparison between our reference profiles and the DSMC profiles obtained for the number density n (a), velocity parallel to the walls u_y (b), as well as for the transversal q_x (c) and longitudinal q_y (d) heat fluxes. Our convention is that the LB results are shown using lines and points, while the corresponding DSMC results are shown for comparison with the same line type, but without points. Despite some visible discrepancies at large Kn in the profiles of n and q_y , the agreement between our simulation results and the DSMC results is excellent, especially for u_y and q_x , where the DSMC and LB results are almost everywhere overlapped. While the profiles of u_y and q_x seem to be independent of the value of Pr , n and q_y are not. The values of Pr at which the presented results were obtained were chosen to match the DSMC results for the temperature profile, as discussed in the following paragraph.

The temperature profiles obtained using our reference LB model are compared with the DSMC results of Ref. [13] in Fig. 3. In plot (a), the temperature profiles at $\text{Kn} = 0.1$ for various values of u_w are shown. The agreement between the LB (lines and points) and

the DSMC (lines) results is excellent. Here, the Prandtl number was set to $\text{Pr} = 0.67$ for $u_w = 0.42$, to $\text{Pr} = 0.685$ at $u_w = 0.63$, while at $u_w = 0.84, 1.26, 1.68$ and 2.1 , we found that a good fit of the LB results to the DSMC data was obtained at $\text{Pr} = 0.695$. In plot (b), the wall velocity is fixed at $u_w = 0.63$ for various values of Kn . We used the following pairs of values $(\text{Kn}, \text{Pr}) \in \{(0.01, 0.67), (0.1, 0.685), (0.25, 0.78), (0.5, 0.9), (1.0, 1.2)\}$. Also represented in this plot is the result in the ballistic regime, where [22]:

$$T_{\text{ballistic}} = \sqrt{T_+ T_-} \left[1 + \frac{4mu_w^2}{3(\sqrt{T_+} + \sqrt{T_-})^2} \right], \quad (4.3)$$

which reduces to $T_{\text{ballistic}} = T_w + mu_w^2/3$ in the case when the plates have equal temperature. The observed agreement is excellent. In plot (c) the wall velocity is taken to be $u_w = 1.26$. The good agreement observed in this case was obtained using $(\text{Kn}, \text{Pr}) \in \{(0.01, 0.67), (0.05, 0.67), (0.25, 0.785), (0.5, 0.98)\}$. Finally, (d) shows the case when $u_w = 2.1$, for which the following values were used: $(\text{Kn}, \text{Pr}) \in \{(0.05, 0.67), (0.1, 0.695), (0.25, 0.785), (0.5, 1.145)\}$.

V. CONVERGENCE TESTS

In order to assess the computational demand for a given level of accuracy while using the mixed lattice Boltzmann models employed in this paper, we perform the convergence test described in Refs. [28, 29]. Before discussing the results, let us briefly summarise the procedure employed for this test.

The convergence test is performed by comparing the macroscopic profiles $M \in \{n, u_y, T, q_x, q_y\}$ obtained with a given model and corresponding reference profiles M_{ref} obtained using a high-order model. Defining the error for the profile M as:

$$\varepsilon_M = \frac{\max_x [|M(x) - M_{\text{ref}}(x)|]}{\Delta M}, \quad (5.1)$$

where $\Delta M = \min\{\max_x [M_{\text{ref}}(x)] - \min_x [M_{\text{ref}}(x)], 0.1\}$, a model is considered to have achieved convergence when the maximum error

$$\varepsilon = \max_M \varepsilon_M \quad (5.2)$$

satisfies the following criterion:

$$\varepsilon < 0.01. \quad (5.3)$$

We have performed the above convergence test for $0.01 \leq \text{Kn} \leq 10^4$ by using a logarithmic scale with twelve points per factor of 10 (i.e. the points 1, 1.2, 1.5, 1.8, 2.2, 2.6, 3.2, 3.8, 4.6, 5.6, 6.8, 8.3, 10 were used between 1 and 10). In our tests we have used three values for Pr and two values for the wall velocities u_w , namely $\text{Pr} \in \{\frac{2}{3}, 1, \frac{4}{3}\}$ and $u_w \in \{0.1, 1.0\}$. The reference profiles were obtained using the $\text{HHLB}(21) \times \text{HLB}(7) \times \text{HLB}(7)$ model, except in the BGK case (when $\text{Pr} = 1$), when the model used for the reference profiles was chosen to be $\text{HHLB}(21) \times \text{HLB}(4) \times \text{HLB}(4)$, as discussed in Sec. III. Our strategy for this convergence test was to construct the profiles relevant to the convergence test (5.3) using all models of type $\text{HHLB}(Q_x) \times \text{HLB}(Q_y) \times \text{HLB}(Q_z)$, where $1 \leq Q_x \leq 21$, while Q_y and Q_z were taken to have equal value given by the minimum between Q_x and either 4 in the BGK case, or 6 when $\text{Pr} \neq 1$, as follows:

$$Q_y = Q_z = \begin{cases} \min(Q_x, 4) & \text{Pr} = 1.0, \\ \min(Q_x, 6) & \text{Pr} \neq 1.0. \end{cases} \quad (5.4)$$

We note that the analysis in Sec. III indicated that the Q_y and Q_z should be set to 7 in order to recover the evolution of the heat flux. However, our numerical experiments have demonstrated that the results obtained using $Q_y = Q_z = 6$ are essentially identical to those corresponding to $Q_y = Q_z = 7$, as long as Q_x is sufficiently large.

The results of the convergence test (5.3) are summarised in Fig. 4. In these plots, the horizontal axis represents Kn in logarithmic scale, while the vertical axis represents the quadrature order Q_{conv} on the x axis (corresponding to the half-range Gauss-Hermite quadrature) required for convergence. It is interesting to see that, for fixed u_w , Q_{conv} does not vary significantly with Pr . The visible differences occur only at large wall velocities ($u_w = 1.0$), where, at small Kn , the recovery of the Navier-Stokes regime requires $Q_y = Q_z = 6$ for the Shakhov collision term, while $Q_y = Q_z = 4$ is sufficient when the BGK case is implemented. It can also be seen that, at fixed Pr and Kn , Q_{conv} increases as u_w is increased.

For the case when $u_w = 0.1$, a relatively small velocity set is required to obtain accurate results throughout the whole spectrum of Kn . Indeed, the model $\text{HHLB}(6) \times \text{HLB}(6) \times \text{HLB}(6)$, which employs a number of $2 \times 6^3 = 432$ velocities, is sufficient to satisfy the 1% convergence test of Eq. (5.3), as can be seen from Fig. 4(a). In fact, for this flow regime, the quadrature orders on the y and z axes can be further reduced to $Q_y = Q_z = 3$, such that the convergence test is satisfied throughout the Kn range with the model

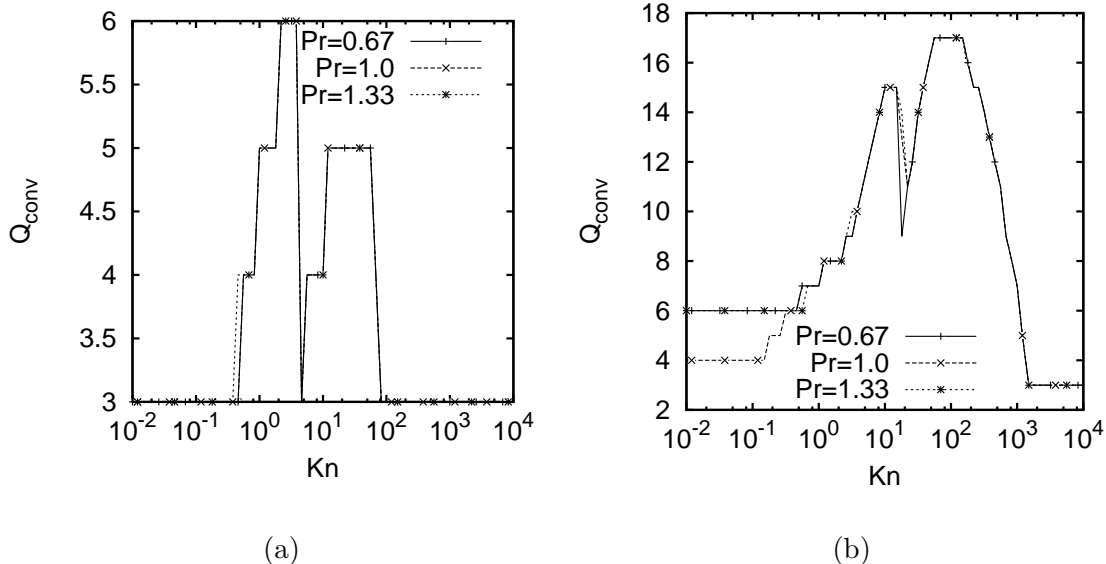


FIG. 4. Quadrature order Q_{conv} on the x axis required to satisfy the convergence test (5.3) for (a) $u_w = 0.1$ and (b) $u_w = 1.0$.

HHLB(6) \times HLB(3) \times HLB(3), which employs only 108 velocities.

VI. CONCLUSION

In this paper, we studied the 3D Couette flow using the mixed quadrature lattice Boltzmann models introduced in Ref. [28] by employing the half-range Gauss-Hermite quadrature on the axis perpendicular to the walls and the full-range Gauss-Hermite quadrature on the two axes which are parallel to the walls.

We first validated our models by comparing the value of the slip velocity obtained for values of the Knudsen number Kn between 0.01 and 100 with the benchmark solution of Ref. [31], as well as with the linearised Boltzmann results reported in Ref. [30]. Furthermore, we compared the particle number density, velocity, temperature and heat flux profiles with the Direct Simulation Monte Carlo (DSMC) results reported in Refs. [9–13]. Here, we found that the hard-sphere results could be successfully recovered by employing the Shakhov collision term, which allows the Prandtl number Pr to be modified. While at small values of the Knudsen number Kn , the value of Pr for hard-sphere particles is $2/3$, the value of

Pr at higher Kn had to be adjusted to fit the DSMC data. In general, we observed good agreement with all of the above data.

Finally, we performed a convergence test with respect to the quadrature order (i.e. the number of velocities). We found that our models can be used to obtain accurate results throughout the whole Kn range (i.e. ranging from the Navier-Stokes regime at $\text{Kn} = 10^{-3}$ up to the ballistic regime). For low-speed flows (i.e. $u_w = 0.1$, corresponding to ~ 23.81 m/s), the $\text{HHLB}(6) \times \text{HLB}(3) \times \text{HLB}(3)$ model (employing $12 \times 3 \times 3 = 108$ velocities) can be used to obtain results which have errors of less than 1% in the profiles of n , u_y , T , q_x and q_y when compared to the reference profiles. In the case when $u_w = 1.0$, errors less than 1% are ensured by the $\text{HHLB}(17) \times \text{HLB}(6) \times \text{HLB}(6)$ model, which employs 1224 velocities.

ACKNOWLEDGEMENTS

This work was supported by a grant of the Romanian National Authority for Scientific Research, CNCS-UEFISCDI, Project No. PN-II-ID-PCE-2011-3-0516. The authors express their gratitude to Prof. Henning Struchtrup (Department of Mechanical Engineering, University of Victoria, Canada) for kindly providing the DSMC results used for the validation of the models introduced in this paper. The authors are grateful to Prof. Li-Shi Luo (Department of Mathematics and Statistics, Old Dominion University, Norfolk, VA) for suggesting the validation of their results using the linearised Boltzmann equation results in Refs. [31, 32].

Appendix A: Non-dimensionalisation of the Boltzmann equation

In order to run our simulations using the same parameters as in the DSMC simulations reported in Ref. [13], the Boltzmann equation was nondimensionalised as follows. In this section, we employ the convention that the quantities before nondimensionalisation are denoted using a tilde $\tilde{\cdot}$. The reference temperature was taken to be $\tilde{T}_{\text{ref}} = 273$ K. Since the authors of Ref. [13] used Argon gas atoms in their simulations, we chose the reference mass to be equal to $\tilde{m}_{\text{ref}} = \tilde{m}_{\text{Ar}} \simeq 6.63 \times 10^{-26}$ kg. The resulting reference velocity is:

$$\tilde{c}_{\text{ref}} = \sqrt{\frac{\tilde{k}_B \tilde{T}_{\text{ref}}}{\tilde{m}_{\text{ref}}}} \simeq 238.35 \frac{\text{m}}{\text{s}}, \quad (\text{A1})$$

where the Boltzmann constant \tilde{k}_B also has a tilde since it is not dimensionless. The average particle number density was taken to be $\tilde{n} = 1.4 \times 10^{20}$ molecules/m³, while the mean free path was chosen as $\tilde{\lambda} = 0.008833$ m. The Knudsen number Kn was controlled by varying the domain size, such that the reference length, reference time and reference densities depend on Kn, as shown in Table I.

The non-dimensional form of the Boltzmann equation can be achieved starting from the Boltzmann equation:

$$\partial_t \tilde{f} + \frac{\tilde{\mathbf{p}}}{\tilde{m}} \tilde{\nabla} f = -\frac{1}{\tilde{\tau}} (\tilde{f} + \tilde{f}^{(\text{eq})}). \quad (\text{A2})$$

First, the non-dimensional distribution function f is defined as:

$$f = \frac{\tilde{f}}{\tilde{n}_{\text{ref}}} (\tilde{m}_{\text{ref}} \tilde{k}_B \tilde{T}_{\text{ref}})^{3/2}, \quad (\text{A3})$$

In the case of the Maxwell-Boltzmann distribution,

$$\tilde{f}^{(\text{eq})} = \frac{\tilde{n}}{(2\pi \tilde{m} \tilde{k}_B \tilde{T})^{3/2}} \exp \left[-\frac{(\tilde{\mathbf{p}} - \tilde{m} \tilde{\mathbf{u}})^2}{2\tilde{m} \tilde{k}_B \tilde{T}} \right], \quad (\text{A4})$$

this procedure yields:

$$f^{(\text{eq})} = \frac{n}{(2\pi m T)^{3/2}} \exp \left[-\frac{(\mathbf{p} - m \mathbf{u})^2}{2m T} \right], \quad (\text{A5})$$

where $\mathbf{p} \equiv \tilde{\mathbf{p}}/\tilde{m}_{\text{ref}}\tilde{c}_{\text{ref}}$. Finally, the Boltzmann equation (A2) can be non-dimensionalised after multiplying both sides by $\tilde{t}_{\text{ref}}(\tilde{m}_{\text{ref}}\tilde{k}_B\tilde{T}_{\text{ref}})^{3/2}/\tilde{n}_{\text{ref}}$, yielding Eq. (2.1). The non-dimensionalised relaxation time τ has the following form [40]:

$$\tau = \frac{\text{Kn}}{n}. \quad (\text{A6})$$

Appendix B: Velocity relaxation in the hydrodynamic limit of the Couette flow

The Navier-Stokes equation reads:

$$\rho[\partial_t \mathbf{u} + (\mathbf{u} \cdot \nabla) \mathbf{u}] = -\nabla P + \frac{1}{3} \eta \nabla(\nabla \mathbf{u}) + \eta \Delta \mathbf{u}, \quad (\text{B1})$$

where a vanishing bulk viscosity and a constant coefficient of shear viscosity μ were considered. To obtain an approximation of the evolution of u_y in the case of the Couette flow, let us consider the case of small wall velocities $\pm u_w$, such that the flow is close to isothermal

Kn	l_{ref}	t_{ref}	n_{ref}
0.01	0.8833 m	3.71 ms	1.24×10^{20} molecules/m ³
0.05	0.17666 m	0.741 ms	2.47×10^{19} molecules/m ³
0.1	0.08833 m	0.371 ms	1.24×10^{19} molecules/m ³
0.25	0.035332 m	0.148 ms	4.95×10^{18} molecules/m ³
0.5	0.017666 m	74.1 μ s	2.47×10^{18} molecules/m ³
1.0	0.008833 m	37.1 μ s	1.24×10^{18} molecules/m ³

TABLE I. Reference values for the length, time and density for various values of Kn.

and incompressible. Thus, $\nabla \mathbf{u} \simeq 0$ and $P = nT$ is constant throughout the channel, such that Eq. (B1) reduces to:

$$\frac{\partial u_y}{\partial t} - \frac{\eta}{\rho} \frac{\partial^2 u_y}{\partial x^2} = 0. \quad (\text{B2})$$

The boundary conditions $u(x = \pm L/2) = \pm u_w$ can be satisfied by considering:

$$u_y(x, t) = \frac{2u_w x}{L} + \tilde{u}_y(x, t), \quad (\text{B3})$$

where $\tilde{u}_y(x = \pm L/2, t) = 0$. Writing $\tilde{u}_y = e^{-\lambda t} U_\lambda(x)$ gives:

$$\frac{\partial^2 U_\lambda}{\partial x^2} + \frac{\rho\lambda}{\eta} U_\lambda = 0. \quad (\text{B4})$$

The solution of the above equation is:

$$U_\lambda(x) = A_\lambda \cos\left(x\sqrt{\rho\lambda/\eta}\right) + B_\lambda \sin\left(x\sqrt{\rho\lambda/\eta}\right). \quad (\text{B5})$$

Assuming that the solution is antisymmetric gives $A_\lambda = 0$, while the parameter λ is constrained such that the sine function vanishes at $x = \pm L/2$:

$$\lambda \rightarrow \lambda_k = \frac{4k^2\pi^2\eta}{\rho L^2}. \quad (\text{B6})$$

Thus, the solution of Eq. (B2) is [41]:

$$u_y = \frac{2u_w x}{L} + \sum_{k=1}^{\infty} e^{-\lambda_k t} a_k \sin \frac{2k\pi x}{L}. \quad (\text{B7})$$

The coefficients a_k can be obtained by requiring that $u_y(x, t = 0) = 0$ (our initial state for this problem):

$$a_k = -\frac{2}{L} \int_{-L/2}^{L/2} dx \frac{2u_w x}{L} \sin \frac{2k\pi x}{L} = \frac{2u_w}{\pi k} (-1)^k. \quad (\text{B8})$$

The following solution is obtained:

$$u_y(x, t) = u_y^{\text{st}}(x) + u_y^{\text{tr}}(x, t), \quad (\text{B9a})$$

where the stationary state solution is $u_y^{\text{st}} = 2u_w x/L$ and the transient part u_y^{tr} is:

$$u_y^{\text{tr}} = \frac{2u_w}{\pi} \sum_{k=1}^{\infty} \frac{(-1)^k}{k} e^{-\lambda_k t} \sin \frac{2k\pi x}{L}. \quad (\text{B9b})$$

Let us estimate the time $t_{1\%}$ required for u_y^{tr} (B9b) to decay to less than 1% of u_w . As $t \rightarrow \infty$, the leading order term $e^{-\lambda_1 t}$ dominates. Requiring that $|a_1|e^{-\lambda_1 t_{1\%}} = 0.01u_w$, where $a_1 = -\frac{2u_w}{\pi}$ (B8), gives:

$$t_{1\%} \simeq \frac{4.154}{\lambda_1}. \quad (\text{B10})$$

The coefficient λ_1 is given by:

$$\lambda_1 = \frac{4\pi^2\eta}{\rho L^2}. \quad (\text{B11})$$

In our simulations, $\rho \simeq 1$, $L = 1$ and $\eta = \tau nT \simeq \text{Kn}$, such that $\lambda_1 \simeq 4\pi^2\text{Kn}$. With this approximation, we obtain

$$t_{1\%} \simeq \frac{0.105}{\text{Kn}}. \quad (\text{B12})$$

In the case when $\text{Kn} = 10^{-3}$ the damping time $t_{1\%} \simeq 105$. Since in this regime, we used $\delta t = 10^{-4}$ per time step, the number of iterations required to achieve $t = t_{1\%}$ is

$$N_{\text{iter}} \simeq 1.05 \times 10^6. \quad (\text{B13})$$

-
- [1] C. Cercignani, *The Boltzmann Equation and Its Applications* (Springer-Verlag, New York, 1988).
 - [2] E. M. Shakhov, *Fluid Dyn.* **3**, 95 (1968).
 - [3] E. M. Shakhov, *Fluid Dyn.* **3**, 112 (1968).
 - [4] J. Y. Yang, J. C. Huang, and L. Tsuei, *Proc. R. Soc. Lond. A* **448**, 55 (1995).
 - [5] Z.-H. Li and H.-X. Zhang, *Int. J. Numer. Meth. Fluids* **42**, 361 (2003).
 - [6] Z.-H. Li and H.-X. Zhang, *J. Comput. Phys* **193**, 708 (2004).
 - [7] Z.-H. Li, H.-X. Zhang, and S. Fu, *Science in China Ser. G* **48**, 496 (2005).
 - [8] Z.-H. Li and H.-X. Zhang, *J. Comput. Phys* **228**, 1116 (2009).

- [9] H. Struchtrup and M. Torrilhon, Phys. Rev. Lett. **99**, 014502 (2007).
- [10] H. Struchtrup and M. Torrilhon, Phys. Rev. E **78**, 046301 (2008).
- [11] M. Torrilhon and H. Struchtrup, J. Comput. Phys. **227**, 1982 (2008).
- [12] P. Taheri, M. Torrilhon, and H. Struchtrup, Phys. Fluids **21**, 017102 (2009).
- [13] A. Schuetze, “*Direct Simulation by Monte Carlo Modeling Couette Flow using dsmclas.f: A user’s manual*,” Report, Department of Mechanical Engineering, University of Victoria, Canada, 2003 (unpublished).
- [14] Z. Guo, “Application of discrete unified gas kinetic scheme for temperature induced non-equilibrium flows,” (2016), the Thirteenth International Conference for Mesoscopic Methods in Engineering and Science ICMMES-2016.
- [15] E. P. Gross, E. A. Jackson, and S. Ziering, Ann. Phys. **1**, 141 (1957).
- [16] S. Lorenzani, L. Gibelli, A. Frezzotti, A. Frangi, and C. Cercignani, Nanoscale and Microscale Thermophysical Engineering **11**, 211 (2007).
- [17] A. Frezzotti, L. Gibelli, and B. Franzelli, Continuum Mech. Thermodyn. **21**, 495 (2009).
- [18] A. Frezzotti, G. P. Ghiroldi, and L. Gibelli, Comput. Phys. Comm. **182**, 2445 (2011).
- [19] L. Gibelli, Phys. Fluids **24**, 022001 (2012).
- [20] Z. Guo, K. Xu, and R. Wang, Phys. Rev. E **88**, 033305 (2013).
- [21] G. P. Ghiroldi and L. Gibelli, J. Comput. Phys. **258**, 568 (2014).
- [22] V. E. Ambruş and V. Sofonea, Phys. Rev. E **89**, 041301(R) (2014).
- [23] V. E. Ambruş and V. Sofonea, Interfac. Phenom. Heat Transfer **2**, 235 (2014).
- [24] V. E. Ambruş and V. Sofonea, Int. J. Mod. Phys. C **25**, 1441011 (2014).
- [25] Z. Guo, R. Wang, and K. Xu, Phys. Rev. E **91**, 033313 (2015).
- [26] G. P. Ghiroldi and L. Gibelli, Commun. Comput. Phys. **17**, 1007 (2015).
- [27] Y. Shi, Y. W. Yap, and J. E. Sader, Phys. Rev. E **92**, 013307 (2015).
- [28] V. E. Ambruş and V. Sofonea, J. Comput. Phys. **316**, 760 (2016).
- [29] V. E. Ambruş and V. Sofonea, J. Comput. Sci. **17**, 403 (2016).
- [30] S. H. Kim, H. Pitsch, and I. D. Boyd, J. Comput. Phys. **227**, 8655 (2008).
- [31] S. Jiang and L.-S. Luo, J. Comput. Phys. **316**, 416 (2016).
- [32] W. Li, L.-S. Luo, and J. Shen, Comput. Fluids **111**, 18 (2015).
- [33] V. A. Titarev, Comput. Fluids **36**, 1446 (2007).
- [34] I. A. Graur and A. P. Polikarpov, Heat Mass Transf. **46**, 237 (2009).

- [35] V. E. Ambruş and V. Sofonea, *Phys. Rev. E* **86**, 016708 (2012).
- [36] F. B. Hildebrand, *Introduction to Numerical Analysis*, second edition ed. (Dover Publications, 1987).
- [37] F. W. J. Olver, D. W. Lozier, R. F. Boisvert, and C. W. Clark, *NIST Handbook of Mathematical Functions* (Cambridge University Press, New York, 2010).
- [38] S. Gottlieb and C.-W. Shu, *Math. Comput.* **67**, 73 (1998).
- [39] O. Rogozin, *Eur. J. Mech. B-Fluid* **60**, 148 (2016).
- [40] Y. Sone, *Molecular Gas Dynamics: Theory, Techniques and Applications* (Birkhäuser, Boston, 2007).
- [41] C. Pozrikidis, *Introduction to Theoretical and Computational Fluid Dynamics* (Oxford University Press, Oxford, 1997).